Regulation of electron transport is essential for photosystem I stability and plant growth

Mattia Storti (iD), **Anna Segalla, Marco Mellon** (iD), **Alessandro Alboresi** (iD) and **Tomas Morosinotto** (iD)

Department of Biology, University of Padova, Padova 35121, Italy

Summary

• Photosynthetic electron transport is regulated by cyclic and pseudocyclic electron flow (CEF and PCEF) to maintain the balance between light availability and metabolic demands. CEF transfers electrons from photosystem I to the plastoquinone pool with two mechanisms, dependent either on PGR5/PGRL1 or on the type I NADH dehydrogenase-like (NDH) complex. PCEF uses electrons from photosystem I to reduce oxygen and in many groups of photosynthetic organisms, but remarkably not in angiosperms, it is catalyzed by flavodiiron proteins (FLVs).

• In this study, *Physcomitrella patens* plants depleted in PGRL1, NDH and FLVs in different combinations were generated and characterized, showing that all these mechanisms are active in this moss.

• Surprisingly, in contrast to flowering plants, *Physcomitrella patens* can cope with the simultaneous inactivation of PGR5- and NDH-dependent CEF but, when FLVs are also depleted, plants show strong growth reduction and photosynthetic activity is drastically reduced.

• The results demonstrate that mechanisms for modulation of photosynthetic electron transport have large functional overlap but are together indispensable to protect photosystem I from damage and they are an essential component for photosynthesis in any light regime.

Introduction

Oxygenic photosynthesis enables plants, algae and cyanobacteria to exploit light to fix carbon dioxide, directly or indirectly supporting the metabolism of most living organisms. In photosynthetic organisms, sunlight powers the linear electron flow (LEF) from water to $NADP^+$ via the activity of two photosystems (PS), PSII and PSI, generating NADPH and ATP to sustain cellular metabolism. Natural environmental conditions are highly variable and sudden changes in irradiation can drastically affect the flow of excitation energy and electrons. The rate of ATP and NADPH consumption is also highly dynamic because of metabolism regulation (Peltier *et al.*, 2010; Allahverdiyeva *et al.*, 2015). Photosynthetic organisms have indeed evolved multiple mechanisms to modulate the flow of excitation energy and electrons according to metabolic constraints and environmental cues, for instance by diverting/feeding electrons from/to the linear transport chain. These mechanisms include the cyclic electron flow (CEF) around PSI, in which electrons are transferred from PSI back to the plastoquinone pool, contributing to proton translocation and ATP synthesis but not to NADPH formation (Joliot & Johnson, 2011; Shikanai, 2014; Shikanai & Yamamoto, 2017). In angiosperms two distinct CEF pathways have been identified: one dependent on a chloroplast NADH dehydrogenase-like (NDH) complex (Shikanai *et al.*, 1998) and the other linked to the presence of PGR5/PGRL1 (Munekage

et al., 2002; DalCorso *et al.*, 2008) (Supporting Information Fig. S1). Although some of the CEF actors have been identified, there is no complete consensus regarding whether PGR5/PGRL1 are directly or indirectly involved in catalyzing electron transport (Hertle *et al.*, 2013; Nawrocki *et al.*, 2019) and to what extent their biological role is due to their activity as stromal electron acceptors or rather as modulators of LEF (Suorsa *et al.*, 2012).

Another alterative electron pathway is pseudocyclic electron flow (PCEF), in which electrons from PSI are used to reduce oxygen (O_2) to water. PCEF is also known as the water–water cycle because H_2O is split by PSII and then resynthesized when O_2 replaces $NADP^+$ as the final electron acceptor downstream of PSI. PCEF includes the Mehler reaction, which is important for detoxifying $O_2^{\cdot-}$ produced by PSI (Asada, 2000) but is estimated to make a limited contribution to electron transport (Driever & Baker, 2011). More recently, enzymes known as flavodiiron proteins (FLVs or FDPs) have been shown to contribute to PCEF (Allahverdiyeva *et al.*, 2013) and to be responsible for significant transient electron transport in *Physcomitrella patens* (Gerotto *et al.*, 2016) (Fig. S1).

CEF and PCEF activities are found in all organisms that perform oxygenic photosynthesis, but the molecular machineries involved are not fully conserved and differ in various phylogenetic groups (Peltier *et al.*, 2010; Ruhlman *et al.*, 2015; Alboresi *et al.*, 2019). In different species of cyanobacteria, unicellular eukaryotic algae and plants, the analysis of specific mutants has

clearly shown that mechanisms for the regulation of photosynthetic electron transport play a key role in the response to dynamic environmental conditions (Suorsa *et al.*, 2012; Yamori & Shikanai, 2016; Shikanai & Yamamoto, 2017). As example, FLVs were shown to play an important role in the response to fluctuating light in different organisms (Allahverdiyeva *et al.*, 2013; Gerotto *et al.*, 2016; Chaux *et al.*, 2017), while PGRL1/PGR5 have important functions under saturating or fluctuating light and anoxia (Munekage *et al.*, 2002; Suorsa *et al.*, 2012; Kukuczka *et al.*, 2014). The inactivation of NDH alone has no major impact on growth and stress responses (Endo *et al.*, 1999; Yamori *et al.*, 2015), although its activity seems to be essential for C_4 metabolism (Ishikawa *et al.*, 2016). All these pathways have a common role in protecting PSI from over-reduction and photoinhibition (Takagi *et al.*, 2016). According to most recent literature, however, this common activity is achieved using different molecular mechanisms. In fact while FLVs act as alternative electron acceptors for PSI, PGR5/PGRL1 was suggested to affect PSI oxidation state indirectly by slowing down the electron flux from Cyt b_6f (Takagi *et al.*, 2017; Yamamoto & Shikanai, 2019; Rantala *et al.*, 2020).

In the present study, we generated mutants defective in CEF and FLVs mechanisms by simultaneously knocking out *pgrl1*, *ndhm* and *flva* in the moss *P. patens*. The results demonstrate strong functional overlap, given that when one protein was depleted its activity was largely compensated for by the others. However, plants with multiple deletions showed very severe phenotypes, demonstrating that the regulation of electron transport is indispensable for PSI stability and plant growth in any conditions, even under weak illumination.

Materials and Methods

Plant material and growth

P. patens (Gransden ecotype) wild-type (WT) and *flva*, *pgrl1* and *ndhm* knockout (KO) lines (Kukuczka *et al.*, 2014; Gerotto *et al.*, 2016; Storti *et al.*, 2019, 2020) were maintained in the protonemal stage by vegetative propagation on $PpNH_4$ medium (Ashton *et al.*, 1979) and grown under controlled conditions: 24°C, 16 h : 8 h, light : dark photoperiod with 50 µmol photons $m^{-2} s^{-1}$ (control light, CL) unless otherwise specified. Physiological and biochemical experiments were performed on 10-d-old plants grown in $PpNO_3$ medium (Ashton *et al.*, 1979). Growth in different media and light regimes (specific conditions are described in the text and in the figure legends) was evaluated starting from protonema colonies of 2 mm in diameter and then followed for 21 d. Colony size was measured as reported in a previous study (Storti *et al.*, 2019). Briefly, high-resolution images (600 ppi) were acquired using a Konica Minolta Bizhub C280 scanner. Images were processed with FIJI (https://fiji.sc/) using the 'threshold colour' plugin to remove the plate background. Finally, integrated density (area × mean density) was measured for each colony and normalized to the WT integrated density under control conditions. This strategy was chosen because growth conditions influence development of moss colonies, from

filamentous tissues developed with a 2D structure (chloronema and caulonema) to 3D gametophore (leafy shoot) and rhizoids (radical-like tissue) (Cove, 2005), which is not take in account by the area.

Pigment analysis

Fresh protonemal tissue (10 d old) was ground with a plastic pestle and pigments were extracted with 80% acetone. The spectra of plant extracts were fitted with those of individual purified pigments to calculate Chla/b and Chl/carotenoid (Chl/Car) ratios (Croce *et al.*, 2002).

Moss transformation and mutant selection

The *pgrl1* (Kukuczka *et al.*, 2014; Gerotto *et al.*, 2016) construct was used to remove the *pgrl1* gene from the *ndhm* single KO genetic background (Storti *et al.*, 2020) to obtain *pgrl1-ndhm* double KO mutants. For triple mutant isolation, the *pgrl1* construct was used to remove *pgrl1* from the *flva-ndhm* background. Similarly, the *ndhm* KO construct (Storti *et al.*, 2020) was used to remove the gene from the *flva-pgrl1* KO background (Storti *et al.*, 2019), obtaining triple *flva-pgrl1-ndhm* KO mutant plants in both cases (Fig. S2). Transformation was performed via protoplast DNA uptake as described by Alboresi *et al.* (2010). Six-day-old protonema cells were treated with driselase (Sigma-Aldrich) to digest the cell wall, and protoplasts were filtered with 100 µm cloth. Protoplasts were washed and resuspend in PEG-4000-containing solution, mixed with linear DNA (10–15 µg) and exposed to heat shock (5 min at 45°C). After 1 d of recovery, protoplasts were first embedded in a top layer solution and plated on agarified medium containing mannitol to prevent their rupture, and then moved to a new plate with antibiotics for mutant selection. After two rounds of selection, the various lines were homogenized using 3 mm zirconium glass beads (Sigma-Aldrich), and genomic DNA (gDNA) was isolated according to a rapid extraction protocol (Edwards *et al.*, 1991) with minor modification. PCR amplification was performed on extracted gDNA (Table S1; Fig. S2). Reverse transcriptase PCR (RT-PCR) was performed on cDNA (RevertAid Reverse Transcriptase; Thermo Scientific, Waltham, MA, USA) synthetized after RNA extraction to confirm the *pgrl1-ndhm* and *flva-pgrl1-ndhm* KO lines.

Spectroscopic analyses

In vivo Chl fluorescence and $P700^+$ absorption were monitored simultaneously at room temperature with a Dual-PAM 100 system (Walz, Effeltrich, Germany) on protonemal tissue grown for 10 d in $PpNO_3$. Before the measurements, the plants were dark-acclimated for 40 min, and the parameter F_v/F_m was calculated as $(F_m - F_0)/F_m$. To determine the induction curves, actinic red light was set at 50 or 540 µmol photons $m^{-2} s^{-1}$, and photosynthetic parameters were recorded every 30 s. At each step, the photosynthetic parameters were calculated as follows: Y(II) as $(F_m' - F_0)/F_m'$; qL as $(F_m' - F)/(F_m' - F_0') \times F_0'/F$; NPQ as $(F_m - F_m')/F_m'$; Y(I) as $1 - Y(ND) - Y(NA)$; Y(NA) as $(P_m - P_m')/P_m$;

Y(ND) as $(P - P_0/P_m)$ (Klughammer & Schreiber, 1994). Electrochromic shift (ECS) spectra were recorded with a JTS-10 system (Biologic, Seyssinet-Pariset, France) in plants that were dark adapted and soaked with 20 mM Hepes, pH 7.5 and 10 mM KCl; the 546 nm background was subtracted from the 520 nm signal, thus eliminating the contribution of cytochromes and scattering effects. Functional photosystem quantification was performed by single flash turnover using a xenon lamp. This lamp can induce PSI double charge separation, and thus PSI/PSII values calculated in this way are overestimated by $c.$ 40% (Gerotto *et al.*, 2016). Samples were infiltrated with 20 µM 3-(3,4-dichlorophenyl)-1,1-dimethylurea (DCMU) and 4 mM HA (hydroxylamine) to eliminate the contribution of PSII (Joliot *et al.*, 2004). Electron transport rate (ETR) was evaluated by DIRK (dark-induced relaxation kinetic, (Sacksteder & Kramer, 2000)) analysis as in Gerotto *et al.* (2016). During 5 min of continuous illumination (940 µmol photons m^{-2} s^{-1}, 630 nm LED) light was switched off at different times (0.24, 0.52, 0.79, 1.07, 1.52, 2.47, 3.93, 6.38, 8.83, 18.88, 48.9, 168.97, 288.99 s) for 20 ms to follow fast decay of the 520 nm ECS component (Slope in the Dark, SD). To measure PSII-independent electron transport, plants were treated with 20 µM DCMU. ETR was calculated as the slope of ECS during light (SL) subtracted from the SD and normalized to the total PS content (PSI + PSII). After 5 min, the light was switched off for 20 s to follow relaxation kinetics and evaluate the proton motive force (pmf) generated during light treatment (Storti *et al.*, 2019). The pmf was determined as the difference of the maximum signal at light steady state and minimum level of ECS in the dark and normalized to total charge separation (PSI + PSII).

Respiration and oxygen evolution

Protonemal tissue grown for 10 d at 50 µmol photons m^{-2} s^{-1} was dark-adapted for 30 min and enclosed in a 2 ml chamber filled with water and supplemented with 10 mM NaHCO$_3$. O$_2$ consumed by respiration in the dark for 10 min at 23°C was measured using a Clark-type O$_2$ electrode (Hansatech, King's Lynn, UK). Gross O$_2$ evolution was measured with the same setup during the exposure of protonemal tissue at 850 µmol photons m^{-2} s^{-1} white light. O$_2$ consumption and evolution rates were normalized to the total Chl content of each sample. Chl content was evaluated after extraction with 80% acetone.

Western blot analysis

Total protein extracts were obtained by grinding protonemal tissues in solubilization buffer (50 mM Tris pH 6.8, 100 mM dithiothreitol, 2% sodium dodecylsulfate and 10% glycerol). Samples were loaded so that the same amount of Chl was present, and after SDS-PAGE, proteins were transferred to a nitrocellulose membrane (Pall Corporation, New York, NY, USA). Membranes were hybridized with specific primary antibodies (anti-PsaA, Agrisera (Vännäs, Sweden), catalog number AS06 172; anti-PsaD, Agrisera, catalog number AS09 461; anti-Cyt f, Agrisera, catalog number AS06 119; anti-γ-ATPase, Agrisera, catalog number AS08 312; custom made anti-FLVA and FLVB (Gerotto

et al., 2016), and custom made anti-D2, anti-CP47, anti-PSBS, anti-LHCSR and anti-NDHM) and detected with alkaline phosphatase conjugated antibody (Sigma Aldrich).

Clear native (CN) gel

Gels were casted in 8 × 10 cm plates using the buffer described by Kügler *et al.* (1997) with an acrylamide gradient of 4–12% in the running gel and 4% acrylamide in the stacking gel. Thylakoids from dark-adapted protonemal tissue were isolated as in Gerotto *et al.* (2012) and resuspended in 25BTH20G (25 mM BisTris-HCl pH 7, 20% glycerol) buffer at 1 µg Chl µl^{-1}. Thylakoids were solubilized as described by Järvi *et al.* (2011), using 0.75% α-DM (α-dodecylmaltoside) and adding deoxycholic acid (DOC 0.2%) to solubilized samples. Anode and cathode buffers were the same used by Järvi *et al.* (2011) for CN gel; the cathode buffer was supplemented with 0.05% DOC and 0.02% α-DM. Gels were run for 4 h with increasing voltage (75–200 V).

Results

Regulation of photosynthetic electron transport is critical for plant growth in any light condition

P. patens plants depleted of FLVA, PGRL1 and NDHM were used as genetic background to generate all combinations of double mutants (*flva-pgrl1*, *flva-ndhm*, *pgrl1-ndhm*) as well as triple *flva-pgrl1-ndhm* KO plants depleted in all three mechanisms in the present study. In all cases, multiple independent lines for each genotype were validated for the correct insertion of the resistance cassettes at the desired loci as well as for the absence of the expression of the corresponding gene. Moreover, triple mutant lines were generated starting from two distinct double-mutant backgrounds (i.e. either *flva-ndhm* or *flva-pgrl1*) to further ensure that the observed plant phenotypes were not due to secondary effects in the selected genetic material (Fig. S2).

Western blotting analysis of proteins of the photosynthetic apparatus confirmed the absence of target proteins such as FLVA and NDHM (Fig. 1a). FLVB was also strongly reduced (*c.* 90% less than in WT) in the absence of FLVA, as expected considering their heteromeric assembly (Allahverdiyeva *et al.*, 2011; Yamamoto *et al.*, 2016). Interestingly, FLVA and FLVB were significantly reduced (70% less than in WT) upon *pgrl1-ndhm* KO as well. No specific antibody was available for PGRL1, but its absence had already been verified by mass spectrometry in the parental *pgrl1* KO lines (Kukuczka *et al.*, 2014). Among the other components of the photosynthetic apparatus, PSI content was reduced, while the relative contents of ATPase, CP47 and PSBS increased in the *flva-pgrl1-ndhm* KO plants. Native PAGE analysis confirmed a clear reduction in PSI-LHCI content in *pgrl1-ndhm* KO plants and especially in the triple *flva-pgrl1-ndhm* KO plants where it was 60% less than in WT (Fig. 1b). The PSI : PSII ratio can also be quantified spectroscopically using the ECS of carotenoid absorption, which is proportional to the number of light-induced charge separations occurring in photosystems (Fig. 1c; Bailleul *et al.*, 2010). This measurement
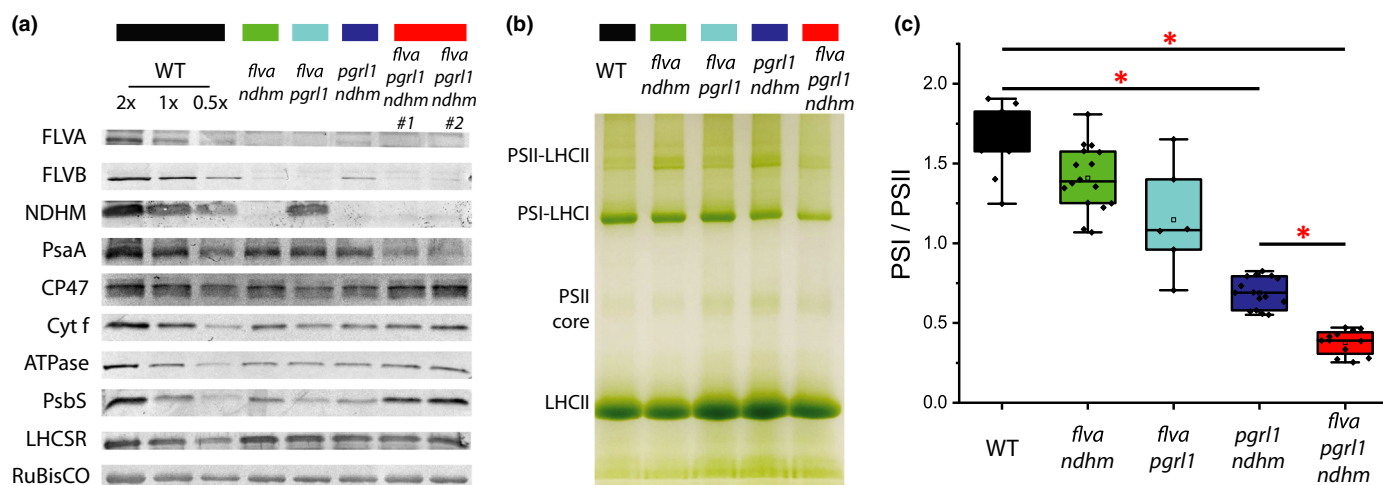
Fig. 1 Impact of mutations on photosynthetic apparatus composition of *Physcomitrella patens*. (a) Immunoblot analysis of various proteins of the photosynthetic apparatus. A total extract amount of proteins equivalent to 2 μg Chl (for FLVB, PsaD, D2, CP47, Cyt f, γATpase, PSBS and LHCSR) and 4 μg Chl (for PSAA, NDHM and FLVA) was loaded for each sample. In the case of the WT, 2× and 0.5× indicate the loading of twice and half the amount of extract, respectively. (b) CN-PAGE (4–12% acrylamide), with thylakoids solubilized with mild detergent (0.75% α-DM). For each lane, a volume of thylakoid membranes corresponding to 15 μg Chl was loaded. (c) PSI : PSII ratio quantified from the ECS signal obtained after the application of a single turnover pulse (see the Materials and Methods section). For each genotype, the average result from two independent lines is reported from a total of $n > 6$ independent biological replicates (one-way ANOVA, $P < 0.001$ is indicated by a red asterisk).

confirmed a strong relative reduction in active PSI in *pgrl1-ndhm* and *flva-pgrl1-ndhm* KO plants. The pigment content was highly similar among the lines, with only a slight but significant decrease in the Chl*a*/*b* content in *flva-pgrl1-ndhm* KO, consistent with a lower PSI content (Table S2).

The impact of the mutations on plant growth was assessed by cultivation on solid medium under different light regimes. All double mutants showed no major defects under nonsaturating light (10–50 μmol photons $m^{-2} s^{-1}$), while differences emerged in more challenging conditions (Figs 2, S3). All plants depleted in PGRL1 showed a growth reduction under intense constant illumination, while all plants depleted in FLVA exhibited less growth when exposed to fluctuating light (FL), as previously reported (Gerotto *et al.*, 2016; Storti *et al.*, 2019). A small growth reduction was also observed in *pgrl1-ndhm* KO plants exposed to light fluctuations, in contrast to both single KO mutants that provided the genetic background (Figs 2, S4). The most striking observation, however, was that *flva-pgrl1-ndhm* triple KO plants showed a 60–75% growth reduction with respect to the WT plants in all conditions, including under very weak, limiting light (10 μmol photons $m^{-2} s^{-1}$). In nonsaturating illumination, the phenotype of the *flva-pgrl1-ndhm* KO plants was thus completely different from those of all the double mutants, highlighting that the mechanisms for the regulation of photosynthetic transport are essential for plant growth.

Such a severe growth phenotype was not present in the rich medium supplemented with 0.5% glucose and 0.05% ammonium tartrate (Fig. 3). The addition of metabolizable sugars such as sucrose or glucose to the basal salt medium was indeed enough to restore plant growth to WT levels (Fig. 3a). Interestingly, however, photosynthetic functionality in these plants was not recovered, and PSI : PSII remained as affected as in phototrophic conditions (Fig. 3c). This suggests that *flva-pgrl1-ndhm* KO mutant growth

impairment is due to a reduced energy supply from photosynthesis. The external carbon source can rescue growth but not the alterations in photosynthetic apparatus. This result also demonstrates the ability of *P. patens* to grow well under mixotrophic metabolism with most of the energy provided by organic substrates, which may be related to adaptation to ecological niches with available decomposing biomass (Graham *et al.*, 2010).

The impact of other environmental parameters affecting photosynthetic metabolism was assessed to further investigate the mechanistic reason for the strong impact on growth. Plants were thus cultivated under saturating CO_2 to stimulate carbon fixation and minimize photorespiration or with 24 h of continuous nonsaturating light to avoid any eventual stress due to dark–light transitions. As shown in Fig. 3(b), both continuous light and high CO_2 induced a slight increase in growth, but the effect was similar in mutant and WT plants. The same experiments were repeated with plants cultivated under very low light for several weeks. In this case, a slight recovery of the growth rate and PSI : PSII ratio was observed, suggesting that PSI is light damaged in *flva-pgrl1-ndhm* KO plants but also that the recovery is extremely slow (Fig. 3c).

CEF and FLVs are fundamental for photosynthetic activity

The mechanistic explanation of the strong growth phenotype observed was investigated by measuring photosynthetic ETR monitoring ECS, following the approach previously employed in different organisms including *P. patens* (Sacksteder & Kramer, 2000; Joliot & Joliot, 2002; Kukuczka *et al.*, 2014). WT plants showed a first peak a few seconds after the light was switched on, largely due to FLV activity (Gerotto *et al.*, 2016), which was consistently absent in all *flva*-less plants (Fig. 4a,b). This first peak was reduced in *pgrl1-ndhm* KO plants but not in the
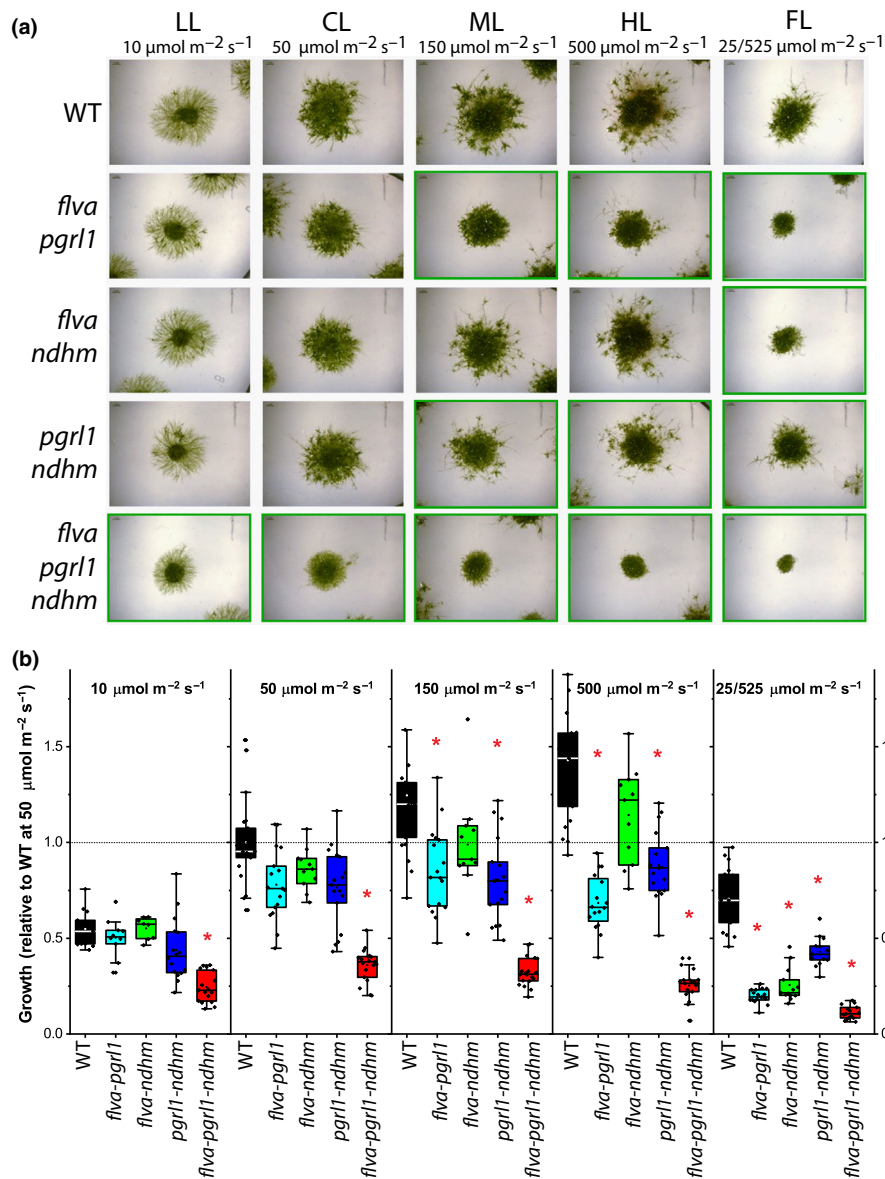
Fig. 2 Impact of the depletion of electron transport regulation on *Physcomitrella patens* growth. WT and mutant plants were grown under illumination of different intensities, ranging from limiting (LL, 10 µmol photons m^{-2} s^{-1}) to optimal (CL, 50 µmol photons m^{-2} s^{-1}) or excessive (ML and HL, 150 and 500 µmol photons m^{-2} s^{-1} respectively). Cells were also exposed to light fluctuations (FL) in which 3 min at 525 µmol photons m^{-2} s^{-1} was followed by 9 min at 25 µmol photons m^{-2} s^{-1}. Representative images (a) and growth quantification (b) of 21-d-old plants. Images of plants showing statistically significantly different growth from the WT are highlighted in green. Examples of growth curves are shown in Supporting Information Fig. S3. In (b), the plot depicts the median and 25–75th percentiles in boxes and the minimum and maximum values as whiskers, with individual data points superimposed on the boxes. WT is shown in black, *flva-pgrl1* in cyan, *flva-ndhm* in green, *pgrl1-ndhm* in blue and *flva-pgrl1-ndhm* in red. Red asterisks indicate genotypes with significant differences from WT when grown under the same conditions (one-way ANOVA, $n = 8$–21, $P < 0.001$).

corresponding single KO mutants (Fig. S4). This finding suggests that in *P. patens* CEF contributes to electron transport upon dark-to-light transition, consistently with observations to a larger extent in *Arabidopsis thaliana* (Munekage *et al.*, 2002).

On longer timescales, ETR increased slowly following the activation of carbon fixation, reaching a steady state after ≈ 3 min. In all double mutants (*flva-pgrl1*, *flva-ndhm*, *pgrl1-ndhm* KO), steady-state ETR was indistinguishable from that in the WT (Fig. 4a,b). These mutants also exhibited a similar capacity to generate a steady-state pmf across the thylakoid membranes (Fig. 4c), as estimated from the ECS signal intensity at steady

state after 5 min of illumination (example in Fig. S5). Oxygen evolution activity (Fig. 4d,e) in all double mutants (*flva-pgrl1*, *flva-ndhm*, *pgrl1-ndhm* KO) was also equivalent to that in the WT, confirming that these plants can all sustain the same photosynthetic activity under stationary conditions. PSII yield of all double mutants was also similar to WT but for *pgrl1-ndhm* (Fig. 4f). The picture was completely different in triple *flva-pgrl1-ndhm* KO plants, in which the ETR capacity was largely reduced even under steady-state photosynthesis after several minutes of illumination (Fig. 4b). The steady-state pmf, its relaxation kinetics after the light was switched off and gross O_2 evolution
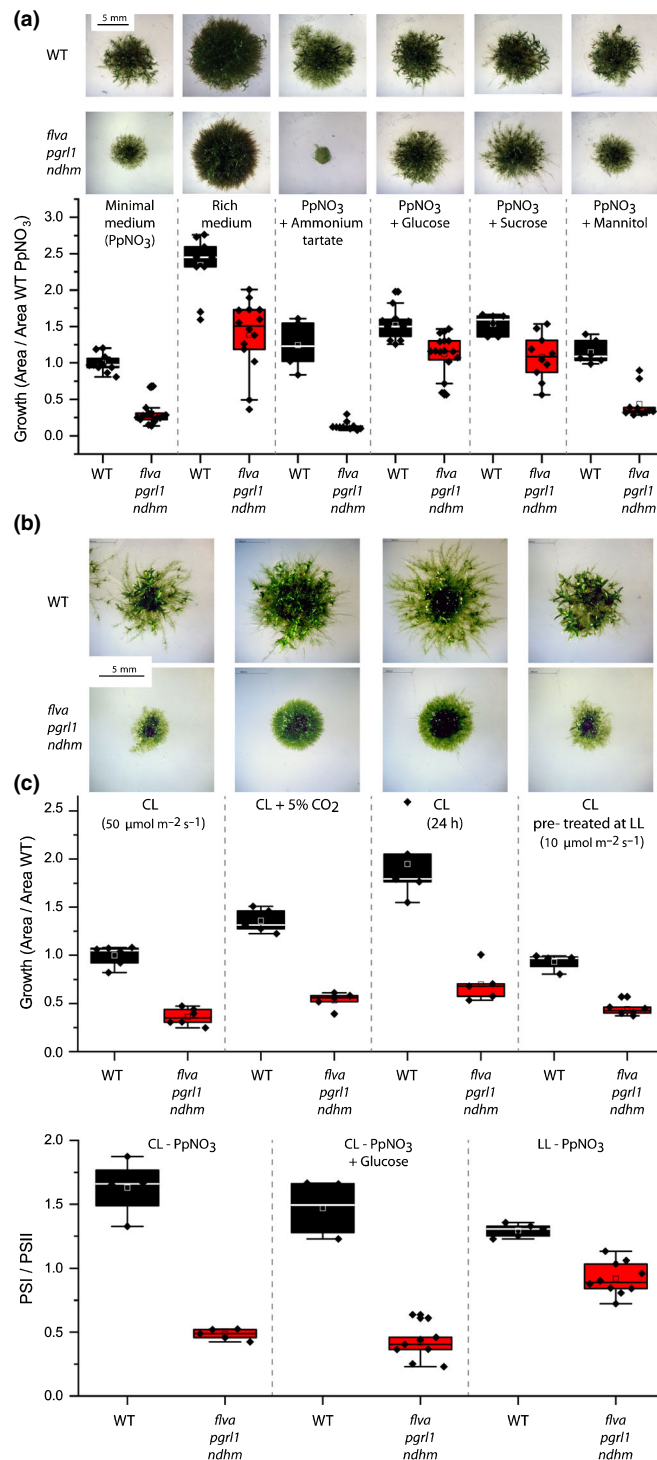
Fig. 3 *Physcomitrella patens* growth and active photosystem content in WT and *flva-pgrl1-ndhm* KO mutants under different conditions. (a) WT and *flva-pgrl1-ndhm* plants were cultivated at 50 μmol photons $m^{-2} s^{-1}$ with different media: minimum medium (PpNO$_3$), rich medium (PpNH$_4$), and minimum medium with the addition of ammonium tartrate (0.05%), glucose (0.5%), sucrose (0.5%) and mannitol (0.5%). (b) WT and *flva-pgrl1-ndhm* KO growth in an atmosphere enriched with 5% CO_2 with 24 h of continuous illumination under control conditions using plants propagated for at least 3 wk under low illumination (LL, 10 μmol $m^{-2} s^{-1}$). In both (a) and (b), growth is normalized to the area of WT plants grown in PpNO$_3$ medium under a 16 h : 8 h, light : dark photoperiod at 50 μmol photons $m^{-2} s^{-1}$. The plot depicts the median and 25–75th percentiles in boxes and the minimum and maximum values as whiskers, with individual data points superimposed on the boxes. For each condition, the WT is shown in black, and *flva-pgrl1-ndhm* KO is shown in red. (c) Spectroscopic quantification of the active PSI : PSII ratio in WT and *flva-pgrl1-ndhm* KO plants cultivated in the presence of glucose and in plants propagated under very low illumination. PSI : PSII should not be considered an absolute quantification, as explained in the Materials and Methods section. For all samples, between four and eight independent biological replicates were performed. The plot depicts the median and 25–75th percentiles in boxes and the minimum and maximum values as whiskers, with individual data points superimposed on the boxes.
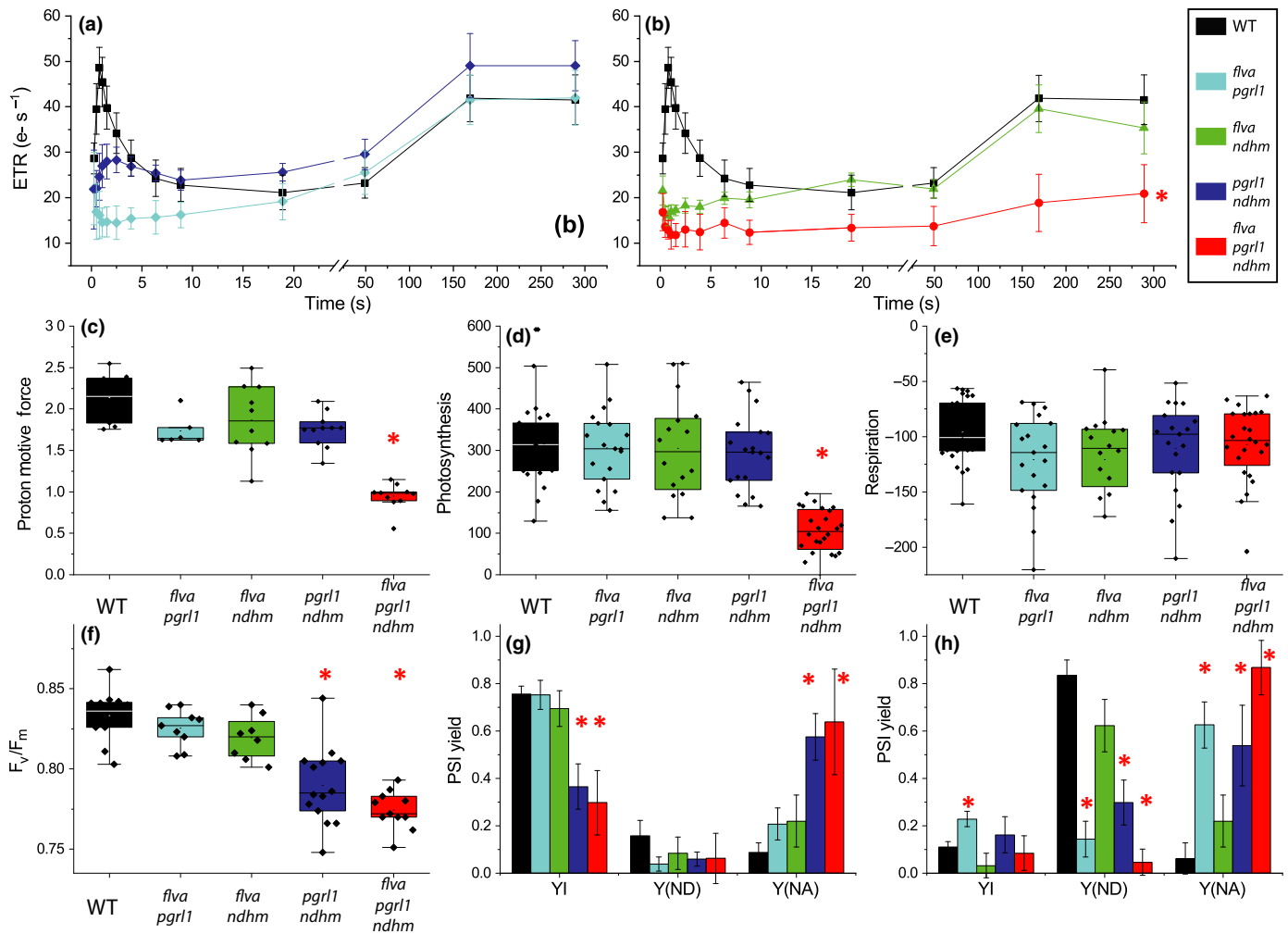
Fig. 4 Photosynthetic electron transfer in *Physcomitrella patens* plants. (a, b) Electron transport rate (ETR) of dark-acclimated plants grown under dim light, calculated from the ECS (electrochromic shift) signal under saturating light (940 µmol photons m^{-2} s^{-1}). Activity was normalized to the total photosystem (PSI + PSII) content. The standard deviation is also reported ($n > 7$). All genotypes were significantly different from WT after 0.8 s of illumination, while only *flva-pgrl1-ndhm* was different from WT after 300 s (*t*-test, $P < 0.01$, indicated by an asterisk). WT data are reported in both (a) and (b) for comparison with other genotypes. (c) Proton motive force (pmf) estimated from the ECS signal at a steady state (after 5 min of illumination). Traces are shown in Supporting Information Fig. S5. *flva-pgrl1-ndhm* was significantly different from WT and all double mutants ($n > 7$). (d) Gross oxygen evolution (nmol O$_2$ min^{-1} mg chl^{-1}) under saturating (800 µmol photons m^{-2} s^{-1}) light. (e) Oxygen consumption in the dark (nmol O$_2$ min^{-1} mg chl^{-1}) measured in dark-acclimated plants. A red asterisk indicates statistical significance (one-way ANOVA, $P < 0.001$, $n > 15$). (f) The PSII quantum yield, as indicated by F_v/F_m, was evaluated in plants cultivated in control conditions (ANOVA, $n > 10$, $P < 0.001$). In (c–f), the 25th and 75th percentiles are delimited by boxes, while whiskers indicate the minimum and maximum values. (g–h) PSI yield, PSI donor (Y ND) and acceptor side (Y NA) limitation upon exposure to limiting (g, 50 µmol photons m^{-2} s^{-1}) or saturating (h, 540 µmol photons m^{-2} s^{-1}) light. The full kinetics are shown in Fig. S7. Data are shown as the average ± SD, and red asterisks indicate values significantly different from those in the WT (one-way ANOVA, $n > 4$, $P < 0.001$). The WT is shown in black, *flva-pgrl1* in cyan, *flva-ndhm* in green, *pgrl1-ndhm* in blue and *flva-pgrl1-ndhm* in red.

during saturating light illumination were also affected, showing that simultaneous depletion of CEF and FLVs had a drastic impact on photosynthetic activity (Figs 4c,d, S5).

CEF activity in *P. patens* is very low (Kukuczka *et al.*, 2014) and detectable only in the first few seconds after light is switched on. Dark-adapted *flv* KO plants showed higher CEF in the first seconds of illumination compared to WT, but it remained low at steady state (Gerotto *et al.*, 2016). *pgrl1-ndhm* and *flva-pgrl1-ndhm* KO plants treated with the PSII inhibitor DCMU showed reduced ETR compared to *flva-pgl1* and *flva-ndhm* KO plants, supporting the idea that both PGRL1 and NDH are involved in this small CEF activity in *P. patens* (Fig. S6).

Saturation pulse analysis to assess PSI quantum yield (Y(I), near infrared spectroscopy) showed that in WT plants exposed to saturating illumination, PSI activity is donor side-limited, as shown by the high Y(ND) (Fig. 4h). In *flva-pgrl1-ndhm* KO plants, by contrast, PSI activity is always acceptor side-limited, as quantified by Y(NA) (Fig. 4g,h). In *flva-pgrl1-ndhm* triple KO plants, PSI and PSII are saturated even under dim illumination (Figs 4g, S7, S8) and show strong PQ over-reduction, as estimated by $1 - qL$, suggesting that electron transport is limited by PSI activity (Fig. S8). Together, these data suggest that the cumulative activity of CEF and FLVs is indispensable to keep the PSI acceptor side oxidized even at very low light intensities.

Discussion

Mechanisms for alternative electron transport play a fundamental biological role despite their apparent limited electron transport capacity

CEF and PCEF regulate photosynthesis in all photosynthetic organisms, and corresponding mutant lines show phenotypes under specific growth conditions such as saturating or fluctuating light (Allahverdiyeva *et al.*, 2013; Peltier *et al.*, 2016; Yamori & Shikanai, 2016). *Arabidopsis* double mutants lacking both CEF activities (specifically *pgr5* and *chlororespiratory reduction/crr* KO plants) show strong growth phenotypes compared to WT (Munekage *et al.*, 2004). Surprisingly, *P. patens* plants depleted of both PGRL1 and NDH can grow as well as the WT under steady illumination (Fig. 2). This capacity can clearly be attributed to the presence of a strong pseudocyclic electron transport mediated by FLVs, absent instead in *Arabidopsis*. In fact, when FLVs are also depleted in the triple *flva-pgrl1-ndhm* KO plants, plant photosynthetic activity is drastically affected even under optimal growth conditions. These results clearly show that FLVs can functionally complement the absence of an active CEF in *pgrl1-ndhm* KO plants and this is achieved even if FLVs are less abundant (Fig. 1) in these plants.

One possible explanation for these observations and the phenotypes of *flva-pgrl1-ndhm* KO plants is that FLVs are complementing the pmf generated by cyclic electron transport. In assessing this hypothesis, however, we should consider that in the angiosperm *Arabidopsis* CEF is estimated to contribute to $\approx 10\%$ of total pmf (Avenson *et al.*, 2005), with a larger role in dark–light conditions or specific developmental stages (Joliot *et al.*, 2004; Allorent *et al.*, 2015). In *P. patens*, the contribution of cyclic electron transport to electron flow is estimated to be even less under steady-state photosynthesis (Kukuczka *et al.*, 2014), with a larger contribution from FLVs and CEF to pmf only being measurable during dark-to-light transitions (Fig. 4) or under peculiar conditions such as anoxia (Kukuczka *et al.*, 2014). Furthermore, these values are estimations of the maximal ETR capacity under saturating illumination, and the actual contribution of these alternative pathways to pmf under limiting light could therefore be even smaller. Overall, in both *A. thaliana* and *P. patens*, according to available data the effect of the inactivation of alternative electron transports would cause a small reduction in the electron transport capacity, which would have only a slight impact on growth if any and, thus, does not explain the strong phenotype of *Arabidopsis pgr5-crr* mutant plants (Munekage *et al.*, 2004) and *P. patens flva-pgrl1-ndhm* KO plants (Figs 2, 3).

These considerations thus suggest that while CEF and FLVs contribute to photosynthetic electron transport, their main biological role is rather to protect PSI from over-reduction and consequent damage (Sonoike, 2011; Tiwari *et al.*, 2016). Such a protection of PSI from over-reduction in the case of FLVs is achieved by activating an alternative electron pathway capable of accepting a significant electron flux from PSI (Fig. 4; Gerotto *et al.*, 2016). In the case of CEF, recent literature has suggested

that PGR5/PGRL1 rather than catalyzing a sustained electron transport they can protect PSI by modulating Cyt b_6f turnover, thus slowing down the ETR to PSI and eventually allowing for re-oxidation of stromal acceptors (Kanazawa *et al.*, 2017; Yamamoto & Shikanai, 2019; Rantala *et al.*, 2020). Despite these mechanistic differences, both FLV and CEF activities result in the increase of PSI donor side limitation, relaxation of the acceptor side limitation and thus protection from over-reduction (Fig. S7).

In the triple *flva-pgrl1-ndhm* KO where all these mechanisms to avoid over-reduction are inactivated, PSI remains limited from the acceptor side (Fig. 4), leading to a decrease in functional PSI (Fig. 1), affecting all photosynthetic activity (Figs 4, S7, S8). It is interesting to observe that the triple *flva-pgrl1-ndhm* KO plants if supplemented with glucose grow as well as the WT, although PSI remains inactivated (Fig. 3) and ETR capacity remains strongly affected (Fig. S9). This suggests that while the supply of organic carbon was able to provide the energy to recover growth, PSI was still damaged under illumination. The long-term impact of PSI inactivation is shown remarkably by the fact that a small recovery in PSI activity was detected in the triple *flva-pgrl1-ndhm* KO plants only with prolonged exposure to a very low light intensity for several weeks (Fig. 3). This extremely slow recovery also indicated that there is not an efficient repair mechanism for PSI, representing a drastic difference from the situation for PSII, which is continuously damaged but also efficiently repaired, as reviewed by Murata *et al.* (2007) and Järvi *et al.* (2015). These data thus point to a protection strategy in which PSII is the main target of light damage in WT plants and is continuously repaired, while PSI remains active even under very strong illumination (Tikkanen *et al.*, 2014). As shown here, however, such a protection strategy is only effective if PSI is indeed very stable because any damage to this complex will have major consequences for growth because of the slow turnover and absence of efficient repair. Hence, PSI needs to be efficiently protected, which is achieved by the presence of multiple, redundant mechanisms that have evolved to ensure its stability under all environmental conditions, as shown in the present study. The results presented also suggest that this role of CEF and FLVs in PSI photoprotection is so important that there cannot be a functioning photosynthesis without at least one functional mechanism, even under extremely low irradiation. If they are completely absent, photosynthesis and plant growth are drastically affected. These nonlinear electron transport pathways are thus not 'simply' regulatory mechanisms that help responses to environmental dynamic changes but rather fundamental components, indispensable for photosynthesis.

Regulation of electron transport adapted during evolution to balance efficiency and photoprotection

Considering their seminal biological role, it is surprising that the full set of photosynthetic electron transport mechanisms is not conserved in all photosynthetic organisms. This is made possible by the presence of multiple pathways with a strong functional

overlap and, if one is lost, the others can compensate for the missing activity. Consistent with this idea is the observation that angiosperms are missing FLVs, but they rely on a stronger CEF (Avenson *et al.*, 2005) to respond to light fluctuations, as shown by the sensitivity of *pgr5/prgl1* KO plants in *Arabidopsis* to these conditions (Suorsa *et al.*, 2012), which is not observed in *P. patens* (Storti *et al.*, 2019). A corollary of this conclusion is also that biological activity is probably underestimated from the analysis of single mutants, the most evident example being the NDH complex. Different plant species (*P. patens* included; Fig. S4) depleted in chloroplast NDH activity show no growth defects under any light conditions and present photosynthetic capacities close to those of WT plants (Peltier *et al.*, 2016; Yamori & Shikanai, 2016). When NDH is depleted from plants already missing other mechanisms, such as in *flva-pgrl1* KO plants here or *pgr5* in *A. thaliana* (Munekage *et al.*, 2004), it instead appears that NDH activity has a strong impact.

FLVs are present and active in cyanobacteria, green algae, mosses and gymnosperms but have been lost by angiosperms and by some secondary endosymbiotic algae, such as diatoms (Shimakawa *et al.*, 2018; Bellan *et al.*, 2020). The most parsimonious hypothesis is that FLVs were present in the prokaryotic cyanobacterial ancestor but were later independently lost in eukaryotes. This implies that FLVs were lost at least twice (in Angiospermae and Heterokonta) during the evolution of photosynthetic organisms, raising the question of whether its activity may have presented a competitive disadvantage in some ecological niches. FLV activity indeed drives energy loss because electrons are donated back to oxygen, generating a futile cycle with water oxidation in PSII. The energy waste is reduced by the regulation of FLV activity, which is maximal only for a few seconds after light fluctuations (Gerotto *et al.*, 2016). Indeed, FLV activity is not detectable during steady-state illumination, and *flv* KO mutants exhibit an ETR that is indistinguishable from that in WT *P. patens* plants (Gerotto *et al.*, 2016). However, this conclusion is challenged by the comparison of *pgrl1-ndhm* KO and *flva-pgrl1-ndhm* KO plants, which differ only in the presence of FLVs. These plants show a highly contrasting phenotype under low steady illumination, demonstrating that FLVs can sustain steady-state activity even in the absence of light fluctuations (Fig. 2), potentially accepting electrons at a low, undetectable rate. This evidence suggests that, even if it is not measurable when CEF is active, FLVs potentially have constant activity under low limiting illumination, where the use of electrons to reduce oxygen to water represents an energy loss and potentially a disadvantage that could drive FLV loss during evolution.

Given the impact on PSI protection and growth when FLVs are depleted, it is reasonable to ask whether FLV introduction in angiosperm crops could potentially lead to increased biomass productivity and yield. While preliminary promising results have been obtained (Wada *et al.*, 2018), some caution is probably necessary because the impact of the genetic modification will probably depend on the species/growing conditions. As discussed, it is in fact possible that FLV activity can cause low but constant energy loss, and thus, improved productivity would be possible only if this is compensated for by increased PSI photoprotection.

According to the present literature, PSI should rarely be damaged in natural conditions, as there are only a few reports of this occurring in some species under specific conditions (Tjus *et al.*, 1998; Sejima *et al.*, 2014). If this is the case and PSI protection mechanisms are indeed very efficient, then the introduction of FLVs should have a limited impact. If, instead, PSI indeed experiences damage, then re-introduction of FLVs should indeed provide an advantage.

Author contributions

TM and AA designed the research. MS, AS, MM and AA performed experiments; MS, AA and TM analyzed the data. TM wrote the paper. All authors reviewed the manuscript.

ORCID

Alessandro Alboresi https://orcid.org/0000-0003-4818-7778
Marco Mellon https://orcid.org/0000-0001-5726-6529
Tomas Morosinotto https://orcid.org/0000-0002-0803-7591
Mattia Storti https://orcid.org/0000-0001-6798-5084

References

Alboresi A, Gerotto C, Giacometti GM, Bassi R, Morosinotto T. 2010. *Physcomitrella patens* mutants affected on heat dissipation clarify the evolution of photoprotection mechanisms upon land colonization. *Proceedings of the National Academy of Sciences, USA* **107**: 11128–11133.

Alboresi A, Storti M, Morosinotto T. 2019. Balancing protection and efficiency in the regulation of photosynthetic electron transport across plant evolution. *New Phytologist* **221**: 105–109.

Allahverdiyeva Y, Ermakova M, Eisenhut M, Zhang P, Richaud P, Hagemann M, Cournac L, Aro E-M. 2011. Interplay between flavodiiron proteins and photorespiration in *Synechocystis* sp. PCC 6803. *Journal of Biological Chemistry* **286**: 24007–24014.

Allahverdiyeva Y, Isojärvi J, Zhang P, Aro E-M. 2015. Cyanobacterial oxygenic photosynthesis is protected by flavodiiron proteins. *Life* **5**: 716–743.

Allahverdiyeva Y, Mustila H, Ermakova M, Bersanini L, Richaud P, Ajlani G, Battchikova N, Cournac L, Aro E-M. 2013. Flavodiiron proteins Flv1 and Flv3 enable cyanobacterial growth and photosynthesis under fluctuating light. *Proceedings of the National Academy of Sciences, USA* **110**: 4111–4116.

Allorent G, Osorio S, Vu JL, Falconet D, Jouhet J, Kuntz M, Fernie AR, Lerbs-Mache S, Macherel D, Courtois F et al. 2015. Adjustments of embryonic photosynthetic activity modulate seed fitness in *Arabidopsis thaliana*. *New Phytologist* **205**: 707–719.

Asada K. 2000. The water–water cycle as alternative photon and electron sinks. *Philosophical Transactions of the Royal Society B: Biological Sciences* **355**: 1419–1431.

Ashton NW, Grimsley NH, Cove DJ. 1979. Analysis of gametophytic development in the moss, *Physcomitrella patens*, using auxin and cytokinin resistant mutants. *Planta* **144**: 427–435.

Avenson TJ, Cruz JA, Kanazawa A, Kramer DM. 2005. Regulating the proton budget of higher plant photosynthesis. *Proceedings of the National Academy of Sciences, USA* **102**: 9709–9713.

Bailleul B, Cardol P, Breyton C, Finazzi G. 2010. Electrochromism: a useful probe to study algal photosynthesis. *Photosynthesis Research* **106**: 179–189.

Bellan A, Bucci F, Perin G, Alboresi A, Morosinotto T. 2020. Photosynthesis regulation in response to fluctuating light in the secondary endosymbiont alga *Nannochloropsis gaditana*. *Plant and Cell Physiology* **61**: 41–52.

Chaux F, Burlacot A, Mekhalfi M, Auroy P, Blangy S, Richaud P, Peltier G. 2017. Flavodiiron proteins promote fast and transient O_2 photoreduction in *Chlamydomonas*. *Plant Physiology* **174**: 1825–1836.

Cove D. 2005. The moss *Physcomitrella patens*. *Annual Review of Genetics* **39**: 339–358.

Croce R, Canino G, Ros F, Bassi R. 2002. Chromophore organization in the higher-plant photosystem II antenna protein CP26. *Biochemistry* **41**: 7334–7343.

DalCorso G, Pesaresi P, Masiero S, Aseeva E, Schünemann D, Finazzi G, Joliot P, Barbato R, Leister D. 2008. A complex containing PGRL1 and PGR5 is involved in the switch between linear and cyclic electron flow in *Arabidopsis*. *Cell* **132**: 273–285.

Driever SM, Baker NR. 2011. The water–water cycle in leaves is not a major alternative electron sink for dissipation of excess excitation energy when CO_2 assimilation is restricted. *Plant, Cell & Environment* **34**: 837–846.

Edwards K, Johnstone C, Thompson C. 1991. A simple and rapid method for the preparation of plant genomic DNA for PCR analysis. *Nucleic Acids Research* **19**: 1349.

Endo T, Shikanai T, Takabayashi A, Asada K, Sato F. 1999. The role of chloroplastic NAD(P)H dehydrogenase in photoprotection. *FEBS Letters* **457**: 5–8.

Gerotto C, Alboresi A, Giacometti GM, Bassi R, Morosinotto T. 2012. Coexistence of plant and algal energy dissipation mechanisms in the moss *Physcomitrella patens*. *New Phytologist* **196**: 763–773.

Gerotto C, Alboresi A, Meneghesso A, Jokel M, Suorsa M, Aro E-MEM, Morosinotto T. 2016. Flavodiiron proteins act as safety valve for electrons in *Physcomitrella patens*. *Proceedings of the National Academy of Sciences, USA* **113**: 12322–12327.

Graham LE, Kim E, Arancibia-Avila P, Graham JM, Wilcox LW. 2010. Evolutionary and ecophysiological significance of sugar utilization by the peat moss *Sphagnum compactum* (Sphagnaceae) and the common charophycean associates *Cylindrocystis brebissonii* and *Mougeotia* sp. (Zygnemataceae). *American Journal of Botany* **97**: 1485–1491.

Hertle AP, Blunder T, Wunder T, Pesaresi P, Pribil M, Armbruster U, Leister D. 2013. PGRL1 is the elusive ferredoxin-plastoquinone reductase in photosynthetic cyclic electron flow. *Molecular Cell* **49**: 511–523.

Ishikawa N, Takabayashi A, Noguchi K, Tazoe Y, Yamamoto H, von Caemmerer S, Sato F, Endo T. 2016. NDH-mediated cyclic electron flow around photosystem I is crucial for C_4 photosynthesis. *Plant and Cell Physiology* **57**: 2020–2028.

Järvi S, Suorsa M, Aro E-M. 2015. Photosystem II repair in plant chloroplasts — Regulation, assisting proteins and shared components with photosystem II biogenesis. *Biochimica et Biophysica Acta (BBA) – Bioenergetics* **1847**: 900–909.

Järvi S, Suorsa M, Paakkarinen V, Aro E-M. 2011. Optimized native gel systems for separation of thylakoid protein complexes: novel super- and mega-complexes. *Biochemical Journal* **439**: 207–214.

Joliot P, Béal D, Joliot A. 2004. Cyclic electron flow under saturating excitation of dark-adapted *Arabidopsis* leaves. *Biochimica et Biophysica Acta* **1656**: 166–176.

Joliot P, Johnson GN. 2011. Regulation of cyclic and linear electron flow in higher plants. *Proceedings of the National Academy of Sciences, USA* **108**: 13317–13322.

Joliot P, Joliot A. 2002. Cyclic electron transfer in plant leaf. *Proceedings of the National Academy of Sciences, USA* **99**: 10209–10214.

Kanazawa A, Ostendorf E, Kohzuma K, Hoh D, Strand DD, Sato-Cruz M, Savage L, Cruz JA, Fisher N, Froehlich JE et al. 2017. Chloroplast ATP synthase modulation of the thylakoid proton motive force: implications for

photosystem I and photosystem II photoprotection. *Frontiers in Plant Science* **8**: 719.

Klughammer C, Schreiber U. 1994. An improved method, using saturating light pulses, for the determination of photosystem I quantum yield via P700+-absorbance changes at 830 nm. *Planta* **192**: 261–268.

Kügler M, Jänsch L, Kruft V, Schmitz UK, Braun HP. 1997. Analysis of the chloroplast protein complexes by blue-native polyacrylamide gel electrophoresis (BN-PAGE). *Photosynthesis Research* **53**: 35–44.

Kukuczka B, Magneschi L, Petroutsos D, Steinbeck J, Bald T, Powikrowska M, Fufezan C, Finazzi G, Hippler M. 2014. Proton gradient Regulation5-Like1-mediated cyclic electron flow is crucial for acclimation to anoxia and complementary to nonphotochemical quenching in stress adaptation. *Plant Physiology* **165**: 1604–1617.

Munekage Y, Hashimoto M, Miyake C, Tomizawa K, Endo T, Tasaka M, Shikanai T. 2004. Cyclic electron flow around photosystem I is essential for photosynthesis. *Nature* **429**: 579–582.

Munekage Y, Hojo M, Meurer J, Endo T, Tasaka M, Shikanai T. 2002. PGR5 is involved in cyclic electron flow around photosystem I and is essential for photoprotection in *Arabidopsis*. *Cell* **110**: 361–371.

Murata N, Takahashi S, Nishiyama Y, Allakhverdiev SI. 2007. Photoinhibition of photosystem II under environmental stress. *Biochimica et Biophysica Acta (BBA) - Bioenergetics* **1767**: 414–421.

Nawrocki WJ, Bailleul B, Cardol P, Rappaport F, Wollman F-A, Joliot P. 2019. Maximal cyclic electron flow rate is independent of PGRL1 in *Chlamydomonas*. *Biochimica et Biophysica Acta (BBA) - Bioenergetics* **1860**: 425–432.

Peltier G, Aro E-M, Shikanai T. 2016. NDH-1 and NDH-2 plastoquinone reductases in oxygenic photosynthesis. *Annual Review of Plant Biology* **67**: 55–80.

Peltier G, Tolleter D, Billon E, Cournac L. 2010. Auxiliary electron transport pathways in chloroplasts of microalgae. *Photosynthesis Research* **106**: 19–31.

Rantala S, Lempiäinen T, Gerotto C, Tiwari A, Aro E-M, Tikkanen M. 2020. PGR5 and NDH-1 systems do not function as protective electron acceptors but mitigate the consequences of PSI inhibition. *Biochimica et Biophysica Acta (BBA) – Bioenergetics* **1861**: 148154.

Ruhlman TA, Chang W-J, Chen JJW, Huang Y-T, Chan M-T, Zhang J, Liao D-C, Blazier JC, Jin X, Shih M-C et al. 2015. NDH expression marks major transitions in plant evolution and reveals coordinate intracellular gene loss. *BMC Plant Biology* **15**: 100.

Sacksteder CA, Kramer DM. 2000. Dark-interval relaxation kinetics (DIRK) of absorbance changes as a quantitative probe of steady-state electron transfer. *Photosynthesis Research* **66**: 145–158.

Sejima T, Takagi D, Fukayama H, Makino A, Miyake C. 2014. Repetitive short-pulse light mainly inactivates photosystem I in sunflower leaves. *Plant and Cell Physiology* **55**: 1184–1193.

Shikanai T. 2014. Central role of cyclic electron transport around photosystem I in the regulation of photosynthesis. *Current Opinion in Biotechnology* **26**: 25–30.

Shikanai T, Endo T, Hashimoto T, Yamada Y, Asada K, Yokota A. 1998. Directed disruption of the tobacco *ndhB* gene impairs cyclic electron flow around photosystem I. *Proceedings of the National Academy of Sciences, USA* **95**: 9705–9.

Shikanai T, Yamamoto H. 2017. Contribution of cyclic and pseudo-cyclic electron transport to the formation of proton motive force in chloroplasts. *Molecular Plant* **10**: 20–29.

Shimakawa G, Murakami A, Niwa K, Matsuda Y, Wada A, Miyake C. 2018. Comparative analysis of strategies to prepare electron sinks in aquatic photoautotrophs. *Photosynthesis Research* **139**: 401–411.

Sonoike K. 2011. Photoinhibition of photosystem I. *Physiologia Plantarum* **142**: 56–64.

Storti M, Alboresi A, Gerotto C, Aro E-M, Finazzi G, Morosinotto T. 2019. Role of cyclic and pseudo-cyclic electron transport in response to dynamic light changes in *Physcomitrella patens*. *Plant, Cell & Environment* **42**: 1590–1602.

Storti M, Puggioni MP, Segalla A, Morosinotto T, Alboresi A. 2020. The activity of chloroplast NADH dehydrogenase-like complex influences the

photosynthetic activity of the moss *Physcomitrella patens*. *bioRxiv*: 2020.01.29.924597.

Suorsa M, Järvi S, Grieco M, Nurmi M, Pietrzykowska M, Rantala M, Kangasjärvi S, Paakkarinen V, Tikkanen M, Jansson S *et al.* **2012.** PROTON GRADIENT REGULATION5 is essential for proper acclimation of *Arabidopsis* photosystem I to naturally and artificially fluctuating light conditions. *The Plant Cell* **24**: 2934–2948.

Takagi D, Ishizaki K, Hanawa H, Mabuchi T, Shimakawa G, Yamamoto H, Miyake C. 2017. Diversity of strategies for escaping reactive oxygen species production within photosystem I among land plants: P700 oxidation system is prerequisite for alleviating photoinhibition in photosystem I. *Physiologia Plantarum* **161**: 56–74.

Takagi D, Takumi S, Hashiguchi M, Sejima T, Miyake C. 2016. Superoxide and singlet oxygen produced within the thylakoid membranes both cause photosystem I photoinhibition. *Plant Physiology* **171**: 1626–1634.

Tikkanen M, Mekala NR, Aro E-M. 2014. Photosystem II photoinhibition-repair cycle protects photosystem I from irreversible damage. *Biochimica et Biophysica Acta (BBA) – Bioenergetics* **1837**: 210–215.

Tiwari A, Mamedov F, Grieco M, Suorsa M, Jajoo A, Styring S, Tikkanen M, Aro EM. 2016. Photodamage of iron–sulphur clusters in photosystem I induces non-photochemical energy dissipation. *Nature Plants* **2**: 16035.

Tjus SE, Møller BL, Scheller HV. 1998. Photosystem I is an early target of photoinhibition in barley illuminated at chilling temperatures. *Plant Physiology* **116**: 755–764.

Wada S, Yamamoto H, Suzuki Y, Yamori W, Shikanai T, Makino A. 2018. Flavodiiron protein substitutes for cyclic electron flow without competing CO_2 assimilation in rice. *Plant Physiology* **176**: 1509–1518.

Yamamoto H, Shikanai T. 2019. PGR5-dependent cyclic electron flow protects photosystem I under fluctuating light at donor and acceptor sides. *Plant Physiology* **179**: 588–600.

Yamamoto H, Takahashi S, Badger MR, Shikanai T. 2016. Artificial remodelling of alternative electron flow by flavodiiron proteins in *Arabidopsis*. *Nature Plants* **2**: 16012.

Yamori W, Shikanai T. 2016. Physiological functions of cyclic electron transport around photosystem I in sustaining photosynthesis and plant growth. *Annual Review of Plant Biology* **67**: 81–106.

Yamori W, Shikanai T, Makino A. 2015. Photosystem I cyclic electron flow via chloroplast NADH dehydrogenase-like complex performs a physiological role for photosynthesis at low light. *Scientific Reports* **5**: 13908.

Supporting Information

Additional Supporting Information may be found online in the Supporting Information section at the end of the article.

Fig. S1 Schematic representation of alternative electron routes.

Fig. S2 Isolation of double and triple KO *Physcomitrella patens* plants.

Fig. S3 Example of growth curve *Physcomitrella patens* mutants.

Fig. S4 Phenotype of *pgrl1* and *ndhm* KO.

Fig. S5 Examples of ECS traces in WT and *flva-pgrl1-ndhm* mutant.

Fig. S6 PSII-independent electron transport.

Fig. S7 PSI functionality under dim/high illumination.

Fig. S8 PSII functionality under dim/high illumination.

Fig. S9 Photosynthetic ETR in plants grown in mixotrophy.

Table S1 Primers used in this work.

Table S2 Pigment composition of *Physcomitrella patens* WT and mutant plants.

Please note: Wiley Blackwell are not responsible for the content or functionality of any Supporting Information supplied by the authors. Any queries (other than missing material) should be directed to the *New Phytologist* Central Office.